

# Alignment-to-orientation conversion and nuclear quadrupole resonance

D. Budker,<sup>1, 2, \*</sup> D. F. Kimball,<sup>1, †</sup> S. M. Rochester,<sup>1, ‡</sup> and J. T. Urban<sup>3, §</sup>

<sup>1</sup>*Department of Physics, University of California at Berkeley, Berkeley, California 94720-7300*

<sup>2</sup>*Nuclear Science Division, Lawrence Berkeley National Laboratory, Berkeley, California 94720*

<sup>3</sup>*Materials Sciences Division, Lawrence Berkeley National Laboratory, and Department of Chemistry, University of California at Berkeley, Berkeley, California 94720-1460*

(Dated: November 2, 2018)

The role of alignment-to-orientation conversion (AOC) in nuclear quadrupole resonance (NQR) is discussed. AOC is shown to be the mechanism responsible for the appearance of macroscopic orientation in a sample originally lacking any global polarization. Parallels are drawn between NQR and AOC in atomic physics.

PACS numbers: 76.60.Gv, 32.80.Bx

The phenomenon of *alignment-to-orientation conversion* (AOC) [1, 2, 3, 4, 5, 6] has been of recent interest to the atomic physics community because it is an important physical mechanism in experiments involving the evolution of atomic ground-state polarization<sup>1</sup> in external fields. In a simple example of atomic AOC, optical pumping by linearly polarized light produces alignment (i.e., the rank-two quadrupole moment, which has a preferred axis but no preferred direction) in an initially isotropic atomic ground state. Application of a static electric field along a direction other than that of the atomic alignment axis induces quantum beats that result in orientation (i.e., the rank-one dipole moment, which has angular momentum biased in one direction).

This Letter draws an analogy between the quadratic Stark splitting encountered in atomic physics experiments and the nuclear quadrupolar coupling encountered in solid-state nuclear quadrupolar resonance (NQR) [7, 8, 9]<sup>2</sup> and nuclear magnetic resonance (NMR) experiments. In particular, we show that in a pulsed NQR experiment, bulk magnetization is created via AOC in an ensemble initially having zero net polarization. We present an analytic calculation of the NQR signal produced by a powder consisting of randomly oriented crystallites and use techniques to visualize nuclear polarization that were developed to aid in the understanding of polarized atomic systems. Given the similarities between atomic physics and NQR/NMR experiments, other opportunities may exist to use knowledge of one of these two well-developed

fields to provide insight into the other, or to aid in the design of new experiments. For example, recent work in atomic physics on the selective creation and detection of various multipole moments [16] could be adapted for use in nuclear systems.

We first describe the relationship between the Stark and nuclear quadrupole Hamiltonians, and then go on to discuss NQR dynamics in more detail. The effect of an electric field  $\vec{E}$ , directed along the quantization axis, on atoms of angular momentum  $F$  is described by the familiar quadratic Stark Hamiltonian:

$$H_{E2} = -\frac{1}{2} \alpha_0 E^2 - \frac{1}{2} \alpha_2 E^2 \frac{3F_z^2 - F(F+1)}{F(2F-1)}. \quad (1)$$

Here  $\alpha_0$  and  $\alpha_2$  are the scalar and tensor electric polarizabilities of the atoms, respectively. The scalar polarizability term causes a uniform shift of all the magnetic sublevels and therefore does not affect the ground-state polarization dynamics. The tensor term of this Hamiltonian is proportional to a rank-two spherical tensor operator  $T_{2,0} = 3F_z^2 - F(F+1)$ . A Hamiltonian consisting of only rank-one terms acts to rotate the system, while a rank-two (or higher) term in the Hamiltonian is generally capable of converting between different rank polarization moments of the system.

Consider a single atomic nucleus with a nonzero quadrupole moment<sup>3</sup> in a polycrystalline solid. While the average electric field “seen” by the nucleus is zero, there may be electric field gradients that interact with the quadrupole moment according to the single-crystallite Hamiltonian (expressed in the Cartesian basis  $x_1 = \hat{x}$ ,  $x_2 = \hat{y}$ ,  $x_3 = \hat{z}$ ) [9]

$$H_Q = -\frac{1}{6} \sum_{i,j} Q_{ij} \frac{\partial E_j}{\partial x_i}. \quad (2)$$

\*Electronic address: budker@socrates.berkeley.edu

†Electronic address: dfk@uclink4.berkeley.edu

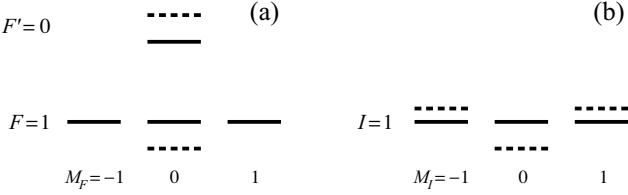
‡Electronic address: simonkeys@yahoo.com

§Electronic address: jurban@ocf.berkeley.edu

<sup>1</sup> Here, we use *polarization* as a generic term describing the anisotropy of a quantum system such as a nucleus or atom. Various types of polarization can be described by *polarization moments* associated with corresponding spherical tensor ranks.

<sup>2</sup> Studies of NQR have intensified in recent years, with NQR in such  $I = 1$  nuclei as  $^{14}\text{N}$  and  $^2\text{H}$  finding applications in, for example, biochemistry [10], and in explosives, land mine, and narcotics detection [11, 12, 13, 14, 15].

<sup>3</sup> In order to possess a quadrupole moment, the nucleus must have angular momentum  $I \geq 1$ . In general, a quantum system with angular momentum  $J$  may have polarization moments of rank  $\kappa$  ranging from 0 to  $2J$ .



Here  $Q_{ij}$  is the nuclear quadrupole moment tensor and  $\vec{E}$  is the local electric field at the position of the nucleus. Upon choosing the Cartesian coordinate system to be the principal axis system of the local electric field gradient (EFG) tensor, this becomes

$$H_Q = \frac{1}{3} \hbar \omega_Q \left\{ [3I_z^2 - I(I+1)] + \frac{\eta}{2} (I_+^2 + I_-^2) \right\}, \quad (3)$$

where

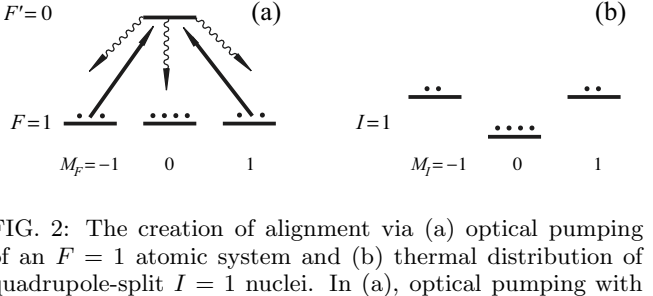
$$\omega_Q = -\frac{3}{4I(2I-1)} \frac{\partial E_z}{\partial z} \langle I, m_I = I | Q_{zz} | I, m_I = I \rangle \quad (4)$$

is the quadrupolar sublevel splitting frequency ( $\langle I, m_I = I | Q_{zz} | I, m_I = I \rangle$  is the nuclear quadrupole moment and  $\partial E_z / \partial z$  is the principal value of the electric field gradient tensor) and the quadrupolar asymmetry parameter is

$$\eta = \frac{\partial E_x / \partial x - \partial E_y / \partial y}{\partial E_z / \partial z}. \quad (5)$$

In the following, we assume  $\eta = 0$ , i.e. that the electric field gradients at each nucleus have cylindrical symmetry about the  $z$ -axis. In this case, the nuclear quadrupole Hamiltonian (Eq. 3) is formally analogous to the atomic Stark Hamiltonian (Eq. 1), with corresponding similarities in both the level splitting (Fig. 1) and the dynamics of the two systems.

The interaction (2) lifts the degeneracy between sublevels corresponding to different magnetic quantum numbers  $|M|$  of the nucleus. In a sample at thermal equilibrium, the energy splitting gives rise to nuclear polarization because, according to the Boltzmann law, there is a higher probability of finding a nucleus in a lower energy state.<sup>4</sup> Thus the nuclear quadrupolar axis is initially along the EFG axis of symmetry. [This is in contrast to



the production of atomic alignment by optical pumping, in which the alignment axis is determined by the polarization of the pumping light (Fig. 2).] Although each nucleus is in an aligned state, in a disordered medium such as a powder there is no macroscopic polarization of the sample because the distribution of individual crystallite orientations is random. However, in spite of this, NQR signals corresponding to macroscopic magnetization of the whole sample can still be observed in such media, as discussed below.

The initial nuclear alignment of several crystallites with different orientations of the local field gradients is illustrated in the first column of Fig. 3 using angular momentum probability surfaces, as discussed in Ref. [17] (see also Ref. [3]). For a particular density matrix, the distance the surface from the origin in a given direction is proportional to the probability of finding the projection  $M = I$  along that direction. For clarity, we assume complete polarization, i.e., that all the nuclei are in the lowest energy state.

The excitation is accomplished by a resonant radiofrequency (rf) magnetic-field pulse. We assume that the field  $\vec{B}(t) = \vec{B}_1 \cos(\omega t + \phi)$  (where  $\omega$  is the rf frequency and  $\phi$  is the rf phase) has constant amplitude  $\vec{B}_1$  and is applied for a time  $\tau$  at an angle  $\beta$  to the EFG axis of symmetry. We assume that  $\omega$  is equal to the quadrupolar frequency  $\omega_Q$ , and consider the decomposition of this field into components along and perpendicular to the EFG axis of symmetry. It can be seen that the longitudinal component causes rapidly oscillating level shifts that have negligible effect on the nuclear polarization, whereas the transverse component can be further decomposed into two oppositely polarized circular components, each of which drives one of the transitions from  $M = 0$  to  $M' = +1$  or  $-1$ . Assuming that the Rabi frequency  $\omega_1 = \gamma B_1$  (where  $\gamma$  is the gyromagnetic ratio) is much less than  $\omega_Q$ , we can neglect the nonresonant component for each transition. The resonant components, of amplitude  $B_1 \sin(\beta)/2$ , cause rotation of the nuclear polarization by an angle  $\omega_1 \tau \sin(\beta)/2$  around the direction of the transverse component of the magnetic field. This follows from

<sup>4</sup> Typical values of the sublevel frequency splittings are between 100 kHz and 10 MHz. At room temperature, the relative population difference between sublevels with different  $|M|$  is typically  $\sim 10^{-7}$ .

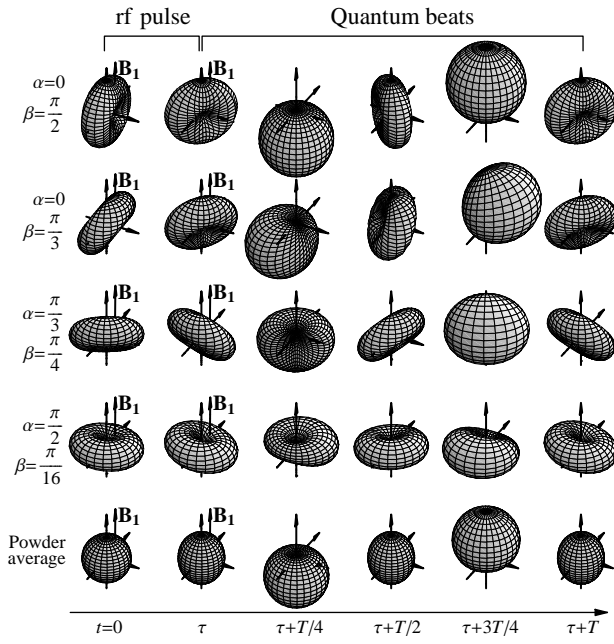


FIG. 3: Probability surfaces [17] corresponding to the evolution of the nuclear polarization in several crystallites with different orientations of the (axially symmetric) local field gradients. The angles  $\alpha$  and  $\beta$  are the Euler angles of the symmetry axes of the local electric field gradients with respect to the fixed lab frame. Each row shows the evolution of a given crystallite in time. The last row shows an average of the polarization over all possible crystallite orientations. The plots at times  $t = 0$  and  $\tau$  show the nuclear polarizations at the beginning and end of the excitation pulse (with magnetic field amplitude  $\vec{B}_1$ ). After the pulse, a quantum beat cycle is shown. As can be seen in the bottom row, macroscopic oscillating orientation appears along the direction of  $\vec{B}_1$ . The plots are generated from a density matrix calculated using an average-Hamiltonian approximation in the quadrupolar interaction frame (see, for example, Ref. [18]). The powder average is found by integrating analytically over the Euler angles (see Appendix).

consideration of the dynamics in an interaction frame in which the quadrupolar interaction is removed and the resonant components of the rf field appear to be static (see Appendix). Since in a typical NQR experiment the pulse length is much longer than the quantum-beat period  $T = 2\pi/\omega_Q$ , quantum beats begin to occur during the rf pulse. However, at times when the quantum-beat phase is zero, the excitation corresponds to simple rotation. In the second column of Fig. 3, we plot only the effect of the rotation, and not of the fast quantum-beat oscillation, by assuming that the pulse length  $\tau$  is an integer number of quantum-beat periods. However, none of the mechanisms described here depend on this assumption. We have chosen the parameters of the excitation pulse such that the rotation is by  $\pi/4$  for crystallites whose EFG axes are orthogonal to the rf polarization

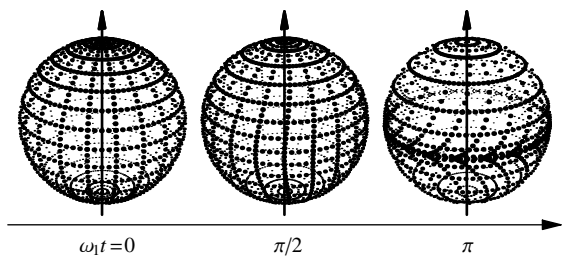


FIG. 4: Dynamics of the individual crystallites' alignment axes during the excitation pulse. Each dot represents the intersection of a crystallite's alignment axis with the unit sphere. Initially ( $\omega_1 t = 0$ ) the alignment distribution is isotropic (dots are plotted along parallels of latitude and meridians of longitude in order to illustrate the dependence of rotation on the initial polar angles). As the phase  $\omega_1 t$  accumulates, the alignment axes rotate (in the average-Hamiltonian approximation) by an angle  $\omega_1 t \sin(\beta)/2$  around the direction of the component of the rf magnetic field transverse to the EFG principal axis, as described in the text. Thus, the alignment axes rotate away from and around the rf field axis (indicated by the vertical arrow).

axis.<sup>5</sup>

After the excitation pulse is over, the alignment axes of the nuclei have been rotated away from the local electric field gradient axes. Thus the nuclei are in coherent superpositions of eigenstates of different energies—the requisite condition for quantum beats. These quantum beats correspond to a cycle of alignment-to-orientation conversion, as shown in the last five columns of Fig. 3. In one period  $T = 2\pi/\omega_Q$  of the cycle, alignment is converted into orientation, then into alignment at an angle of  $\pi/2$  with respect to the original alignment, followed by conversion to the opposite orientation, and back to the original state. This evolution is the same as the evolution of an aligned atomic system in the presence of an electric field (see, for example, Ref. [17]).

The powder average over all crystallites is shown in the bottom row of Fig. 3. Initially ( $t = 0$ ) the sample has no average polarization, as indicated by the isotropic probability surface. At the end of the excitation pulse of length  $\tau$  (where  $\tau$  is chosen to be an integer multiple of  $T$ ) there

<sup>5</sup> According to common NMR/NQR terminology, the pulse that accomplishes such a rotation is called a  $\pi/2$  pulse. The terminology stems from the two-level spin-1/2 system, where if one starts, for example, with a “spin-down” state and applies a pulse creating a coherent superposition of “spin-down” and “spin-up” states (with equal amplitudes of the two components) this corresponds to rotating the orientation direction by  $\pi/2$ . Similarly, a  $\pi$  pulse transfers all atoms from the spin-down state to the spin-up state, and rotates the orientation by  $\pi$ . In the present case of a spin-one system, if the excitation pulse transfers all of the initial  $M = 0$  population into a superposition of the  $M = \pm 1$  sublevels, this actually corresponds to a physical rotation of the alignment by  $\pi/2$  (not by  $\pi$ !). Unfortunately, there appears to be some confusion in the literature about this point.

is a net nuclear alignment within the sample, indicated by the elongation of the probability surface along the  $\vec{B}_1$  axis. The net alignment arises because the alignment axis of each nucleus rotates away from the  $\vec{B}_1$  axis during the excitation pulse (Fig. 4). Following the excitation pulse, each nucleus undergoes alignment-to-orientation conversion. Since the orientation produced in each crystallite is perpendicular to both the EFG principal axis and the axis of the alignment prepared by the excitation pulse, all crystallites contribute coherently to the orientation along  $\vec{B}_1$ , which leads to a net oscillating orientation<sup>6</sup> of the entire sample. This oscillating orientation corresponds to a net sample ac magnetization that is the source of the detected NQR signal. Details of the calculation used to obtain the powder-averaged dynamics, including an analytic formula for the powder-averaged density matrix, are given in the Appendix.

It must be mentioned that the conversion between polarization moments of quadrupolar nuclei is well understood in the field of nuclear magnetic resonance in the context of multiple-quantum coherences. The NMR situation differs from that of NQR in several respects. At the high magnetic field strengths common in NMR experiments, the interaction of the nuclear spin system with this field is dominant. Within the rotating frame approximation, the quadrupolar interaction for any crystallite appears to be cylindrically symmetric about the external magnetic field axis, and the applied resonant rf fields are transverse and appear to be static in the rotating frame. Additionally, the nuclear spin system is initially magnetized (oriented) along the dominant magnetic field direction. When the rf irradiation is weak compared to the quadrupolar interaction, the conversion of orientation to alignment has been recognized as the means by which multiple-quantum coherence can be created from nuclear spin magnetization during a single pulse [19, 20]. When strong, short rf pulses are used, during which quadrupolar evolution is negligible, the multipolar (polarization moment) formalism has shown how multiple-quantum coherence can be created after a two-pulse sequence via orientation-to-alignment conversion due to quadrupolar evolution between the pulses [21, 22]. Furthermore, methods have been introduced to visualize the polarization moments of the nuclear spin system in terms of graphical representations of the corresponding spherical harmonics [23].

<sup>6</sup> Even though each crystallite is undergoing alignment-to-orientation conversion, the sample as a whole has only oscillating orientation and no oscillating alignment. Since the system is symmetric about the  $\vec{B}_1$  axis, all polarization not along  $\vec{B}_1$

Finally, we mention that various techniques for converting nuclear alignment into orientation have been developed for the studies of nuclear moments of short-lived nuclides [24, 25].

In conclusion, we have shown that alignment-to-orientation conversion plays a prominent role in the phenomenon of nuclear quadrupole resonance, converting local nuclear alignment into global orientation, and thus causing the appearance of a macroscopic oscillating magnetic moment. This has been illustrated using the method of angular momentum probability surfaces, and the relationship of this mechanism to that of AOC in atomic physics has been discussed. In future work, it will be interesting to extend the present analysis to NQR and NMR in nuclei with  $I > 1$ , for which polarization moments higher than alignment are possible and the transformations between these moments during quantum beats are more complicated than alignment-to-orientation conversion [17, 26].

The authors are grateful to A. Trabesinger for the suggestion to explore the connection between atomic physics and NQR, and to him and S. J. Freedman, J. Granwehr, A. Pines, V. V. Yashchuk, and M. Zolotorev for useful discussions. This work has been supported by the Office of Naval Research (grant N00014-97-1-0214), by NSF, and by the Director, Office of Science, Office of Basic Energy Sciences, Materials Sciences and Nuclear Science Divisions, of the U.S. Department of Energy under contract DE-AC03-76SF00098. D.B. also acknowledges the support of the Miller Institute for Basic Research in Science.

## APPENDIX A: THEORY

The Hamiltonian governing the NQR dynamics in the presence of an rf field is derived, for example, in Ref. [18]. It is convenient to represent this Hamiltonian in the  $(|x\rangle, |y\rangle, |z\rangle)$  Cartesian basis<sup>7</sup> of the EFG principal axis system (oriented at Euler angles  $\alpha$  and  $\beta$  to the rf field), because the nuclear quadrupolar Hamiltonian (3) is diagonal in this basis. Transforming to the quadrupolar interaction frame removes the diagonal nuclear quadrupolar Hamiltonian and adds additional time-dependent terms in the off-diagonal elements. This form of the Hamiltonian, given by

averages to zero.

<sup>7</sup> Defined by  $|x\rangle = (|M = -1\rangle - |M = +1\rangle)/\sqrt{2}$ ,  $|y\rangle = -i(|M = -1\rangle + |M = +1\rangle)/\sqrt{2}$ ,  $|z\rangle = |M = 0\rangle$ .

$$\hat{H}(t) = \hbar\omega_1 \cos(\omega t + \phi) \begin{pmatrix} 0 & \cos \beta e^{\frac{2in}{3}\omega_Q t} & \cos \alpha \sin \beta e^{i(1+\frac{\eta}{3})\omega_Q t} \\ \cos \beta e^{-\frac{2in}{3}\omega_Q t} & 0 & i \sin \alpha \sin \beta e^{i(1-\frac{\eta}{3})\omega_Q t} \\ \cos \alpha \sin \beta e^{-i(1+\frac{\eta}{3})\omega_Q t} & -i \sin \alpha \sin \beta e^{-i(1-\frac{\eta}{3})\omega_Q t} & 0 \end{pmatrix}, \quad (A1)$$

facilitates a low-power time-average approximation that removes rapidly oscillating terms. Assuming that the electric field gradients are cylindrically symmetric ( $\eta = 0$ ) and that the rf field is resonant with the quadrupolar frequency ( $\omega = \omega_Q$ ), upon averaging over time-dependent terms the Hamiltonian becomes

$$\bar{H}(t) = \frac{\hbar\omega_1}{2} \begin{pmatrix} 0 & 0 & \cos\alpha\sin\beta e^{-i\phi} \\ 0 & 0 & i\sin\alpha\sin\beta e^{-i\phi} \\ \cos\alpha\sin\beta e^{i\phi} & -i\sin\alpha\sin\beta e^{i\phi} & 0 \end{pmatrix}. \quad (\text{A2})$$

We assume that the initial density matrix (also written in the Cartesian basis) is fully aligned along the EFG axis:

$$\rho(0) = \begin{pmatrix} 0 & 0 & 0 \\ 0 & 0 & 0 \\ 0 & 0 & 1 \end{pmatrix}. \quad (\text{A3})$$

The interaction-frame time dependence is given by

$$\begin{aligned} \tilde{\rho}(t) &= e^{-i\bar{H}t/\hbar} \rho(0) e^{i\bar{H}t/\hbar} \\ &= \begin{pmatrix} \cos^2\alpha\sin^2(\frac{1}{2}\omega'_1 t) & -i\cos\alpha\sin\alpha\sin^2(\frac{1}{2}\omega'_1 t) & -\frac{i}{2}\cos\alpha\sin(\omega'_1 t)e^{-i\phi} \\ i\cos\alpha\sin\alpha\sin^2(\frac{1}{2}\omega'_1 t) & \sin^2\alpha\sin^2(\frac{1}{2}\omega'_1 t) & \frac{1}{2}\sin\alpha\sin(\omega'_1 t)e^{-i\phi} \\ \frac{i}{2}\cos\alpha\sin(\omega'_1 t)e^{i\phi} & \frac{1}{2}\sin\alpha\sin(\omega'_1 t)e^{i\phi} & \cos^2(\frac{1}{2}\omega'_1 t) \end{pmatrix}, \end{aligned} \quad (\text{A4})$$

where  $\omega'_1 = \omega_1 \sin\beta$ . In order to find the dynamics of the powder average, we transform out of the interaction frame and rotate the coordinate system to coincide with the lab frame, with  $\vec{B}_1$  along the quantization axis. The algebraic form of the resulting density matrix is complicated. However, since in the powder the only preferred

direction is along  $\vec{B}_1$ , the powder average will be symmetric about this axis. Thus, if we represent the density matrix in the  $(| -1 \rangle, | 0 \rangle, | 1 \rangle)$  Zeeman basis, the averaged density matrix will be diagonal, and we can ignore the off-diagonal terms:

$$\rho_{\text{Lab}}(t) = \frac{1}{8} \begin{pmatrix} 3 - \cos\omega'_1 t - (1 + \cos\omega'_1 t)\cos 2\beta + 4\sin\omega'_1 t \sin\beta \sin(\omega t + \phi) & \dots & \dots \\ \dots & 8\cos^2(\frac{1}{2}\omega'_1 t)\cos^2\beta & \dots \\ \dots & \dots & 3 - \cos\omega'_1 t - (1 + \cos\omega'_1 t)\cos 2\beta - 4\sin\omega'_1 t \sin\beta \sin(\omega t + \phi) \end{pmatrix}. \quad (\text{A5})$$

To obtain the result for the powder as a whole, we average over the Euler angles, evaluating the integrals using *Mathematica* software:

$$\begin{aligned} \rho_{\text{avg}}(t) &= \frac{\int_0^{2\pi} d\alpha \int_0^\pi \rho_{\text{Lab}}(t) \sin\beta d\beta}{\int_0^{2\pi} d\alpha \int_0^\pi \sin\beta d\beta} \\ &= \frac{1}{24} \begin{pmatrix} 10 + 4F'(-\frac{1}{4}\omega_1^2 t^2) - 3\pi\mathbf{H}_{-1}(\omega_1 t) + 8F''(-\frac{1}{4}\omega_1^2 t^2)\omega_1 t \sin(\omega t + \phi) & 0 & 0 \\ 0 & 4 + 4F'''(-\frac{1}{4}\omega_1^2 t^2) & 0 \\ 0 & 10 + 4F'(-\frac{1}{4}\omega_1^2 t^2) - 3\pi\mathbf{H}_{-1}(\omega_1 t) - 8F''(-\frac{1}{4}\omega_1^2 t^2)\omega_1 t \sin(\omega t + \phi) & 0 \end{pmatrix}. \end{aligned} \quad (\text{A6})$$

Here

$$F'(z) = {}_1F_2\left[(2); \left(\frac{1}{2}, \frac{5}{2}\right); z\right], \quad F''(z) = {}_1F_2\left[(2); \left(\frac{3}{2}, \frac{5}{2}\right); z\right], \quad F'''(z) = {}_1F_2\left[(1); \left(\frac{1}{2}, \frac{5}{2}\right); z\right], \quad (\text{A7})$$

${}_pF_q[\mathbf{a}; \mathbf{b}; z]$  is the generalized hypergeometric function

where

$${}_pF_q[\mathbf{a}; \mathbf{b}; z] = \sum_{k=0}^{\infty} \frac{(a_1)_k \dots (a_p)_k}{(b_1)_k \dots (b_q)_k} \frac{z^k}{k!}, \quad (\text{A8})$$

$$(c)_n = c(c+1)\dots(c+n-1) \quad (\text{A9})$$

is the Pochhammer symbol, and  $\mathbf{H}_n(z)$  is the Struve function, which satisfies the differential equation

$$z^2 y'' + zy' + (z^2 - n^2) y = \frac{2}{\pi} \frac{z^{n+1}}{(2n-1)!!}, \quad (\text{A10})$$

where

$$n!! = n(n-2)(n-4)\dots \quad (\text{A11})$$

represents the double factorial.

This gives the powder average during the rf pulse. The terms proportional to  $\sin(\omega t + \phi)$  represent the quantum beats at the quadrupolar splitting frequency. In order to find the evolution after the pulse, we set the factors  $\omega_1 t$  to a constant corresponding to the phase accumulated during Rabi oscillation induced by the excitation pulse. In the results presented here, we set this constant equal to  $\pi/2$ . The only remaining time dependence is then in the  $\sin(\omega t + \phi)$  terms.

---

[1] M. Lombardi, J. Phys. (Paris) 30 (8-9) (1969) 631.  
[2] R. Hilborn, L. Hunter, K. Johnson, S. Peck, A. Spencer, J. Watson, Phys. Rev. 50 (3) (1994) 2467.  
[3] M. Auzinsh, Can. J. Phys. 75 (12) (1997) 853.  
[4] D. Budker, D. F. Kimball, S. M. Rochester, V. V. Yashchuk, Phys. Rev. Lett. 85 (10) (2000) 2088.  
[5] J. Alnis, M. Auzinsh, Phys. Rev. A 63 (2) (2001) 023407/1.  
[6] M. C. Kuntz, R. Hilborn, A. M. Spencer, Phys. Rev. A 65 (2) (2002) 023411.  
[7] T. P. Das, E. L. Hahn, Nuclear quadrupole resonance spectroscopy, Solid state physics. Supplement 1, Academic, New York, 1958.  
[8] H. Kopfermann, Nuclear moments, Academic Press, New York, 1958.  
[9] A. Abragam, The principles of nuclear magnetism, International series of monographs on physics, Clarendon, Oxford, 1962.  
[10] D. T. Edmonds, C. P. Summers, J. Mag. Reson. 12 (2) (1973) 134.  
[11] J. P. Yesinowski, M. L. Buess, A. N. Garraway, M. Ziegeleid, A. Pines, Anal. Chem. 67 (13) (1995) 2256.  
[12] M. D. Rowe, J. A. S. Smith, Mine detection by nuclear quadrupole resonance, in: EUREL International Conference. The Detection of Abandoned Land Mines: A Humanitarian Imperative Seeking a Technical Solution, IEE, Conf. Publ. No. 431, London, UK, 1996, p. 62.  
[13] A. N. Garraway, M. L. Buess, J. B. Miller, B. H. Suits, A. D. Hibbs, G. A. Barrall, R. Matthews, L. J. Burnett, IEEE Transactions on Geoscience and Remote Sensing 39 (6) (2001) 1108.  
[14] V. S. Grechishkin, A. A. Shpilevoi, Phys. Usp. 39 (7) (1996) 713.  
[15] V. S. Grechishkin, N. Y. Sinyavskii, Phys. Usp. 40 (4) (1997) 393.  
[16] V. V. Yashchuk, D. Budker, W. Gawlik, D. F. Kimball, Y. P. Malakyan, S. M. Rochester, physics/0302079, to appear in Phys. Rev. Lett. (2003).  
[17] S. M. Rochester, D. Budker, Am. J. Phys. 69 (4) (2001) 450.  
[18] Y. K. Lee, Concepts in Magnetic Resonance 14 (3) (2002) 155.  
[19] S. Vega, T. W. Shattuck, A. Pines, Phys. Rev. Lett. 37 (1) (1976) 43.  
[20] S. Vega, A. Pines, J. Chem. Phys. 66 (12) (1977) 5624.  
[21] B. C. Sanctuary, T. K. Halstead, P. A. Osment, Mol. Phys. 49 (4) (1983) 753.  
[22] G. J. Bowden, W. D. Hutchison, J. Mag. Reson. 67 (3) (1986) 403.  
[23] T. K. Halstead, P. A. Osment, B. C. Sanctuary, J. Mag. Reson. 60 (3) (1984) 382.  
[24] K. Matsuta, T. Minamisono, Y. Nojiri, M. Fukuda, T. Onishi, K. Minamisono, Nucl. Instrum. Methods A 402 (1998) 229.  
[25] N. Coulier, G. Neyens, S. Teughels, D. L. Balabanski, R. Coussement, G. Georgiev, S. Ternier, K. Vyvey, W. F. Rogers, Phys. Rev. C 59 (4) (1999) 1935.  
[26] G. J. Bowden, W. D. Hutchison, J. Khachan, J. Mag. Reson. 67 (3) (1986) 415.